

Influence of hydrodynamic interactions on lane formation in oppositely charged driven colloids

M. Rex^a and H. Löwen

Institut für Theoretische Physik II: Weiche Materie, Heinrich-Heine-Universität Düsseldorf, Universitätsstraße 1, D-40225 Düsseldorf, Germany

Received 13 September 2007 and Received in final form 7 January 2008

Published online: 6 March 2008 – © EDP Sciences / Società Italiana di Fisica / Springer-Verlag 2008

Abstract. The influence of hydrodynamic interactions on lane formation of oppositely charged driven colloidal suspensions is investigated using Brownian dynamics computer simulations performed on the Rotne-Prager level of the mobility tensor. Two cases are considered, namely sedimentation and electrophoresis. In the latter case the Oseen contribution to the mobility tensor is screened due to the opposite motion of counterions. The simulation results are compared to that resulting from simple Brownian dynamics where hydrodynamic interactions are neglected. For sedimentation, we find that hydrodynamic interactions strongly disfavor laning. In the steady state of lanes, a macroscopic phase separation of lanes is observed. This is in marked contrast to the simple Brownian case where a finite size of lanes was obtained in the steady state. For strong Coulomb interactions between the colloidal particles a lateral square lattice of oppositely driven lanes is stable similar to the simple Brownian dynamics. In an electric field, on the other hand, the behavior is found in qualitative and quantitative accordance with the case of neglected hydrodynamics.

PACS. 82.70.Dd Colloids – 61.20.Ja Computer simulation of liquid structure – 64.70.D- Solid-liquid transitions – 05.70.Ln Nonequilibrium and irreversible thermodynamics

1 Introduction

The dynamics of colloidal particles dispersed in a fluid solvent is quite different from the ballistic motion of molecular systems which is described by Newton's law [1–4]. The viscous solvent both damps the motion of a colloidal particle and leads to kicks of the solvent molecules with the colloidal particle leading to Brownian motion if the time-scales of the molecular solvent is much faster than that of the diffusive motion of the colloidal particles. In concentrated suspensions, a dragged colloidal particle influences the motion of other particles via the solvent flow field. These so-called hydrodynamic interaction is typically long-ranged. While it can be neglected in colloidal suspensions of very small volume fractions, it induces significant corrections in the equilibrium and nonequilibrium dynamics of colloidal suspensions [3,5]. The equilibrium structures and phase boundaries, on the other hand, are unaffected by hydrodynamic interactions.

In the past years a simple nonequilibrium phase transition [6–9] has been discussed in a binary mixture of colloidal particles which are driven by a constant external field [10–13]. The drive is different on the two particle

species and could arise from gravity and from an external electric field in the case of charged colloidal suspensions. Brownian dynamics computer simulations with neglected hydrodynamic interactions strongly support the scenario that — as a function of the driving strength — the mixtures undergoes a transition from a mixed steady state with anisotropic correlations towards a steady state where macroscopic lanes are formed. The transitions has been found for oppositely driven repulsive mixtures [10–16] in two and three spatial dimensions and it seems to be a first-order nonequilibrium transition with a significant hysteresis in an order parameter which detects laning [10]. The general scenario occurs also in pedestrian dynamics [17,18] and in granular matter [19,20]. The formation of columnar and globular structures in bidisperse sedimentation generated solely by hydrodynamic backflow was reported by Batchelor and Janse van Rensburg already in 1986 [21].

Recently, lane formation was observed in real-space experiments by Leunissen *et al.* [22]. Equimolar mixtures of oppositely charged colloidal particles were prepared which form binary ionic crystals [23,24]. These crystals were exposed to a strong external electric field and the dynamics of lane formation was watched by confocal microscopy. Subsequently extensive Brownian dynamics

^a e-mail: rexm@thphy.uni-duesseldorf.de

simulations were carried out to map the nonequilibrium phase diagram [25]. These simulations assumed a Yukawa pair interaction between the particles and neglected hydrodynamic interactions completely. A wealth of different steady-state structures was detected. In particular different orderings were found in the plane perpendicular to the drive including a square, triangular or rhombic crystalline lattice of lanes, a network structure with a finite structural length and intermediate chain formation of lanes [25]. A rough estimate of the experimental parameters used in reference [22] reveals that the laned state observed experimentally indeed falls into the region where laning is expected to occur by Brownian-dynamics computer simulations.

In this paper we address the question how hydrodynamic interactions influence the scenario and the steady-state diagram of lane formation. Our motivation to do so is twofold: First, the experiments, of course, contain hydrodynamic interactions in their full glory, and therefore an inclusion of hydrodynamic interactions is needed for a quantitative comparison. Second, there is a principal need to understand in which direction hydrodynamics influence lane formation. In particular it is known [26] that the leading long-ranged term in the mobility pair tensor is screened if an electric field is applied since a charged colloidal particle is surrounded by counterions of opposite charge. That makes the hydrodynamic interaction significantly different from, *e.g.*, sedimentation induced by different buoyant masses of oppositely charged colloids where the action of gravity on the microions can safely be neglected. In the latter case, the leading part in the mobility tensor at large interparticle separation is the *unscreened* Oseen tensor. It would be interesting to explore how far the steady state is affected by hydrodynamic interactions in both cases of sedimentation and electrophoresis.

We use Brownian-dynamics computer simulations and include hydrodynamic interaction by using mobility tensors on the Rotne-Prager level. Both cases of sedimentation and electrophoresis are studied separately with an unscreened, respectively, screened version of the mobility tensor. The steady-state phase diagrams and the drift velocity are simulated. The simulation data are compared to that obtained by simple Brownian dynamics where hydrodynamic interactions are neglected. For sedimentation, we find that hydrodynamic interactions strongly disfavor laning. In the steady state of lanes, a macroscopic phase separation of lanes is observed, *i.e.* the sickness of the lanes are of the system size. This is in marked contrast to the simple Brownian case where a finite size of lanes was obtained in the steady state. For strong Coulomb interactions between the colloidal particles a lateral square lattice of oppositely driven lanes is stable similar to the simple Brownian dynamics. In an electric field, on the other hand, the behavior is found in qualitative and quantitative accordance with the case of neglected hydrodynamics. All lateral structures are reproduced and the topology of the steady-state phase diagram is unchanged.

The paper is organized as follows: in Section 2, we describe our model and simulation scheme for sedimentation and electrophoresis. Brownian dynamics simula-

tion results are presented in Section 3. We conclude in Section 4.

2 The model

We perform Brownian-dynamics simulations to study an equimolar binary mixture of $2N = 1024$ oppositely charged colloidal particles of diameter σ dissolved in a solvent fluid of shear viscosity η at temperature T and volume fraction $\phi = 2N\pi\sigma^3/6l^3$ exposed to an external driving field, where l is the dimension of a cubic simulation box having periodic boundary conditions. Henceforth, σ serves as the unit of length and $k_B T$, the thermal energy, as the energy unit of the system. To mimic the experiments by Leunissen *et al.* [22,27] the particles interact with an effective screened Coulomb potential (or Yukawa potential) [28] plus a steric repulsion V_h :

$$V(r_{ij}) = V_0 \frac{Z_i Z_j}{(1 + \kappa\sigma/2)^2} \frac{e^{(-\kappa\sigma(r_{ij}/\sigma - 1))}}{r_{ij}/\sigma} + V_h(r_{ij}), \quad (1)$$

with $V_0 = 50k_B T$ the strength of the interaction potential and $Z_i = \pm 1$ the sign of the charge of particle i . $r_{ij} = |\mathbf{r}_i - \mathbf{r}_j|$ denotes the distance between particle i and j , where \mathbf{r}_i is the coordinate vector. The inverse screening length κ governs the range of the interaction and is determined by the salt concentration of the solution. The steric repulsion between the particles, that prevents the system from collapsing, is approximated by a repulsive (shifted and truncated) Lennard-Jones potential

$$V_h(r_{ij}) = \begin{cases} \epsilon \left[\left(\frac{\sigma}{r_{ij}} \right)^{12} - \left(\frac{\sigma}{r_{ij}} \right)^6 + \frac{1}{4} \right], & \text{if } r_{ij} \leq 2^{1/6}\sigma, \\ 0, & \text{else,} \end{cases} \quad (2)$$

with $\epsilon = 4V_0/(1 + \kappa\sigma/2)^2$. The constant external driving field that acts in opposite directions on the two different particle species reads as

$$\mathbf{F}_i^{\text{ext}} = Z_i f \mathbf{e}_z, \quad (3)$$

where \mathbf{e}_z is the unit vector along the z -direction and $f = 150k_B T/\sigma$ is the strength of the external force. The external force is supposed to stem from either an electric field or a gravitational field accompanied with different buoyant masses of the oppositely charged particles. Though the external force, equation (3), may in both cases be identical, if the charges and/or buoyant masses are chosen accordingly, the hydrodynamic interactions are not.

The algorithm used to simulate the diffusive Brownian motion of the colloidal particles was proposed by Ermak and McCammon [29]. Here, the translational displacements of the particles are deemed to occur in time steps of fixed length Δt and the update algorithm is given by [30]

$$\mathbf{r}_i(t + \Delta t) = \mathbf{r}_i(t) + \Delta t \sum_{j=1}^N \left\{ \frac{\mathbf{D}_{ij}(t)}{k_B T} \cdot \mathbf{F}_j(t) + \nabla_{\mathbf{r}_j} \cdot \mathbf{D}_{ji}(t) \right\} + \Delta \mathbf{r}_i^G, \quad (4)$$

where \mathbf{D}_{ij} denotes the diffusion tensor field depending on the positions of the particles at time t . The random displacements $\Delta\mathbf{r}_i^G$ are chosen from a joint Gaussian distribution with mean and covariant matrix [30]

$$\langle\Delta\mathbf{r}_i^G\rangle_G = 0; \quad \langle\Delta\mathbf{r}_i^G\Delta\mathbf{r}_j^G\rangle_G = 2\mathbf{D}_{ij}\Delta t, \quad (5)$$

where $\langle\dots\rangle_G$ denotes the average over the Gaussian noise distribution. $\mathbf{F}_i(t)$, $i = 1, \dots, N$, comprises the nonhydrodynamic forces due to interparticle interactions, determined by the gradient of the interaction potentials in equations (1) and (2), and the external force $\mathbf{F}_i^{\text{ext}}$, equation (3), acting onto particle i .

Hydrodynamic interactions are included in the simulation through the mobility tensor $\boldsymbol{\mu}_{ij} = \mathbf{D}_{ij}/k_B T$. In a first approach we neglect hydrodynamic interactions completely to assess its effect on the system. In that case the diffusion tensor is given by Stoke's law in diagonal form

$$\gamma\boldsymbol{\mu}_{ij} = \delta_{ij}\mathbf{1}, \quad (6)$$

with friction $\gamma = 3\pi\eta\sigma_H$, where σ_H is the hydrodynamic diameter. In the sedimentation and electrophoresis situation we approximate the mobility tensor by two-body interactions. In this approximation the divergence in equation (4) vanishes always [31]. When studying the sedimentation, the buoyant masses of the oppositely charged particles are supposed to be such that the same force acts on the two species but in opposite directions. The action of gravity on the microions can safely be neglected. Therefore, in sum no net force is acting on the solvent and overall it remains quiescent. Then, for a pair of spheres of hydrodynamic diameter σ_H the mobility tensor is approximated by the well-known Rotne-Prager expression [32]

$$\gamma\boldsymbol{\mu}_{ij}^{\text{RP}} = \delta_{ij}\mathbf{1} + (1 - \delta_{ij}) \left[\frac{3\sigma_H}{8}\mathbb{O}(\mathbf{r}_{ij}) + \frac{\sigma_H^3}{16}\mathbb{Q}(\mathbf{r}_{ij}) \right], \quad (7)$$

where

$$\mathbb{O}(\mathbf{r}) = \frac{1}{|\mathbf{r}|}(\mathbf{1} + \hat{\mathbf{r}} \otimes \hat{\mathbf{r}}); \quad \mathbb{Q}(\mathbf{r}) = \frac{1}{|\mathbf{r}|^3}(\mathbf{1} - 3\hat{\mathbf{r}} \otimes \hat{\mathbf{r}}), \quad (8)$$

with the unit vector $\hat{\mathbf{r}} = \mathbf{r}/|\mathbf{r}|$, \otimes a dyadic product, and δ_{ij} Kronecker's symbol. On this level of approximation we incorporate all interactions up to $O((\sigma_H/r)^3)$. Higher-order contributions such as many-body, coupling between rotational and translational motions, and lubrication forces are neglected. The leading term in equation (7) is given by $\mathbb{O}(\mathbf{r})$ which is of the order of $1/|\mathbf{r}|$ for large distances.

However, when regarding the electrophoresis the mobility tensor has to be altered since forces induced by the surrounding counterions into the solvent are in sum equal to the force induced by a colloidal particle. Thus, the solvent flow stemming from the drag on the counterions cannot be neglected as is done in the sedimentation case. It results in an effective screening of the leading far-distance term of the hydrodynamic interactions between the colloidal particles as Long and Ajdari have shown [26]. Their

mobility tensor $\boldsymbol{\mu}_{ij}^{\text{LA}}$ reads as

$$\begin{aligned} \gamma\boldsymbol{\mu}_{ij}^{\text{LA}} = & \delta_{ij}\mathbf{1} + \frac{3\sigma_H}{4}(1 - \delta_{ij}) \\ & \times \left[\frac{e^{-\kappa r_{ij}}}{r_{ij}} \left(\left(1 + \frac{1}{\kappa r} + \frac{1}{\kappa^2 r^2} \right) \mathbf{1} \right. \right. \\ & \left. \left. - \left(\frac{1}{3} + \frac{1}{\kappa r} + \frac{1}{\kappa^2 r^2} \right) 3\hat{\mathbf{r}}_{ij} \otimes \hat{\mathbf{r}}_{ij} \right) - \frac{1}{\kappa^2} \mathbb{Q}(\mathbf{r}_{ij}) \right]. \quad (9) \end{aligned}$$

Here, the leading-order term is $\mathbb{Q}(\mathbf{r}_{ij})$ which decays as $1/|\mathbf{r}^3|$.

Some further remarks concerning the use of the far-field mobility tensors $\boldsymbol{\mu}_{ij}^{\text{RP}}$ and $\boldsymbol{\mu}_{ij}^{\text{LA}}$ are in order. Both are in general justified only for particles separated by several diameters. Furthermore, in the derivation of $\boldsymbol{\mu}_{ij}^{\text{LA}}$ the off-diagonal entries relate the force on a pointlike (colloid) charge, immersed in an infinite undisturbed electrolyte solution, to the resulting change in the fluid velocity at a vector distance \mathbf{r} . Thereby, the charge density distribution is described on the Debye-Hückel level that is suited for weakly charged point ions. The distortion of the spherical electrolyte atmosphere around the colloidal particle by the electric field is neglected. For high volume fractions and large screening length, where particles are close to contact and the counterion clouds overlap, the above mobility tensor is therefore likely to be inaccurate. We acknowledge that both mobilities are crude and questionable approximations to the true ones and should therefore be regarded just as a first step in including hydrodynamic interactions properly. However, to some extent the problems are overcome by the fact that the considered colloidal particles are coated with a polymer layer. To account for this polymer coating, that gives rise to the steric repulsion, we choose $\sigma_H = 0.9\sigma$ throughout this paper. As a result, this ensures the positive definiteness of both mobility tensors since configurations with $|\mathbf{r}_i - \mathbf{r}_j| \leq \sigma_H$ are of negligible statistical weight.

More sophisticated simulation techniques for spherical particles in an unbounded space including lubrication approximation for particles in close proximity and multipolar expansion methods are available [33–37]. However, in the electrophoresis where the hydrodynamic interactions of the counterions become important explicit simulations of all colloidal particles and their counterions — 110 per colloidal particle in the experiments by Leunissen *et al.* — are still beyond computational means. Therefore, we adopted the calculations of Long and Ajdari to our simulations and compare it to the sedimentation problem on the same level of accuracy, *i.e.* the Rotne-Prager level. To our best knowledge this is the first Brownian-dynamics simulations with the Long and Ajdari mobility term 9. Though the interaction strength for low salt concentrations and the external force are large against the thermal energy with a Péclet number of $\text{Pe} = f\sigma/k_B T = 150$, we perform Brownian-dynamics simulation to prevent particles from crystallizing within a lane.

Both mobility tensors, equations (7) and (9), are long-ranged and thus require an Ewald-like summation in simulations analogous to Coulomb and dipole-dipole

interactions. Details on the summation and discussions about appropriate boundary conditions to the system can be found elsewhere [38–41]. We applied the scheme suggested by Beenakker [41] and adapted it for μ_{ij}^{LA} accordingly, *i.e.*, only the dipolar part is used with the simple modification $a^3 \rightarrow -3a\kappa^{-2}$, where $a = \sigma_H/2$. The square root of the diffusion tensor, needed when calculating the random displacements in equation (5), are obtained from a Cholesky decomposition:

$$\mathbf{D} = \mathbf{L} \cdot \mathbf{L}^T, \quad (10)$$

where \mathbf{L} is a lower triangular matrix and \mathbf{L}^T is its transpose. A suitable time scale for our system is $\tau_B = \gamma\sigma^2/k_B T$. The equations of motion including the external field are numerically solved using a finite time step $\Delta t = 2 \cdot 10^{-5} \tau_B$ in all simulations. Statistics were gathered after an initial relaxation period of $20\tau_B$. The starting configuration of all simulations was a homogeneous mixture.

3 Results

3.1 Order parameter and steady-state phase diagrams

To assess the effect of hydrodynamic interactions on the lane behavior of oppositely charged colloidal particles we study a set of volume fractions ϕ and inverse screening lengths $\kappa^* = \kappa\sigma$ and map out nonequilibrium steady-state phase diagrams for all three situations: hydrodynamic interactions neglected (A), electrophoresis (B), and sedimentation (C).

A state of lane is thereby identified by a laning order parameter that is defined through

$$\Phi = \frac{1}{2N} \left\langle \sum_{i=1}^{2N} \Phi_i \right\rangle_t, \quad (11)$$

where the angular brackets $\langle \dots \rangle_t$ denote a time average. The local order parameter $\Phi_i = (n_1 - n_o)^2 / (n_1 + n_o)^2$ is assigned to every particle i , where the numbers n_1 and n_o are the number of like charged particles and oppositely charged particles, respectively, whose projections of distance onto the plane perpendicular to the field are smaller than a suitable cut-off length scale z_c . Φ_i is equal to 1 if all particles within this distance criterion are of the same kind and zero if $n_1 = n_o$, *i.e.* a homogeneous mixture. We chose for convenience $z_c = \frac{3}{4}\sigma$ to detect all lanes starting from a single queue of particles. In what follows we will use a threshold: for $\Phi \geq 1/2$ we call the configuration a state of lanes while in the opposite case ($\Phi < 1/2$) we call it a state without lanes.

We observe that lanes form different structures in the plane perpendicular to the driving direction for different values of κ^* and ϕ . We find lanes placed on a square or triangular lattice, a network-like structure (reminiscent of a bicontinuous microemulsion or microphase-separated system), coexistence regimes of the same, and

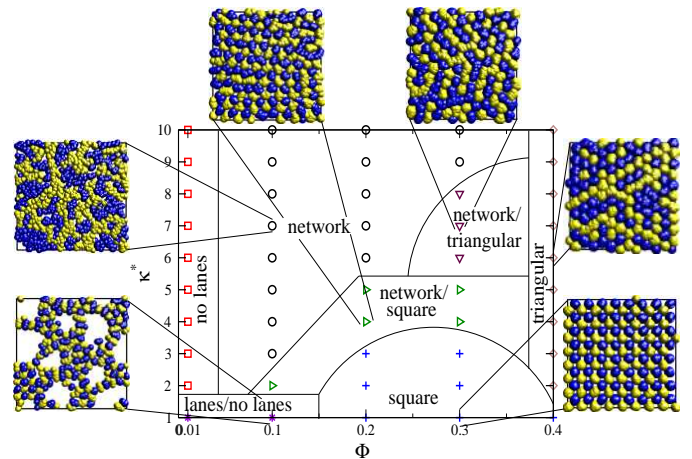


Fig. 1. (Color online) Nonequilibrium steady-state phase diagram for a constant driving force of strength $f = 150k_B T / \sigma$ with hydrodynamic interactions neglected accompanied by a typical simulation snapshot of the projection of the particle coordinates onto the plane perpendicular to the driving field for each different state. The lines between the phases are a guide for the eye.

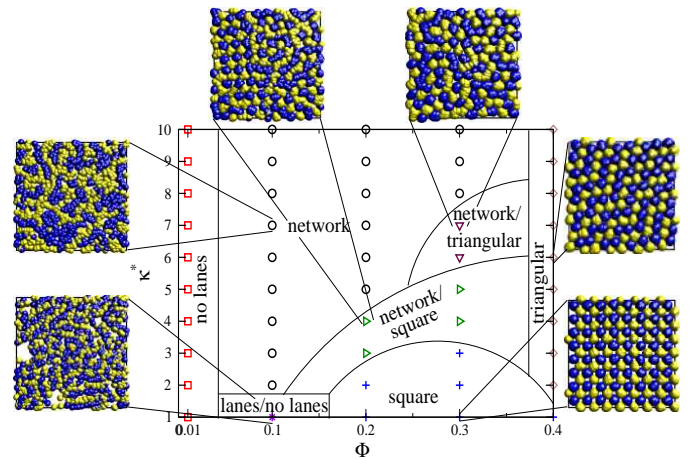


Fig. 2. (Color online) Same as Figure 1 but for electrophoresis with hydrodynamic interactions taken into account through μ_{ij}^{LA} in equation (9). The phase diagram reveals only minor differences as compared to the case of neglected hydrodynamic interactions in Figure 1.

macroscopically separated lanes. The resulting nonequilibrium steady-state phase diagrams are shown in Figures 1, 2, and 3. They are accompanied with typical simulation snapshots of the projection of all particle coordinates onto the xy -plane of the respective situation.

What can be seen at first sight is that the qualitative behavior of situation (A) and (B) in Figures 1 and 2 is almost identical with only subtle differences, while, on the other hand, the phase behavior changes drastically for situation (C), Figure 3. In the latter the whole phase diagram is altered and the diversity of phases found is reduced compared to the first two cases.

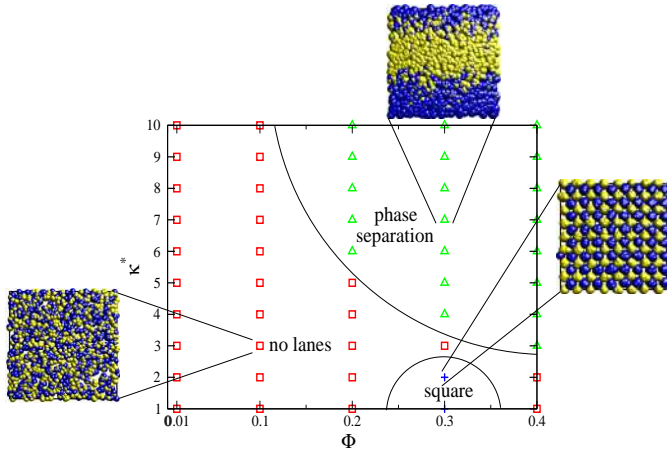


Fig. 3. (Color online) Same as Figure 1 but for sedimentation with hydrodynamic interactions taken into account through μ_{ij}^{RP} in equation (7). The phase diagram shows significant changes as compared to Figure 1 and Figure 2.

3.2 Comparison of simulation results for neglected hydrodynamic interactions and electrophoresis

In this subsection we briefly describe the two phase diagrams in Figures 1 and 2 and their differences, beginning at low volume fractions and ending at high ones, and then dwell on the third diagram, Figure 3, thereafter in subsection 3.3. A more ample discussion on how different phases are identified and what structural correlations they exhibit can be found in a previous work of the authors on the same system with hydrodynamic interactions neglected but for a slightly different driving strength and larger systems [25]. Here, we find for situation (A) virtually the same results as in the previous work with only one difference, namely that we do not encounter a rhombic phase for $\phi = 0.4$ and $\kappa^* = 1, 2, 3$.

For very low volume fraction, $\phi \lesssim 0.01$, in both systems the correlations between the particles are not sufficient to form lanes at all. Thus, the systems are in a phase of no-lanes. Only for very low salt concentration, *i.e.* small κ^* , where the electrostatic coupling between the colloidal particles is strong, we find a coexistence region between lanes and no-lanes. Here, the region with no-lanes consists of voids, where hardly any particle is found. The structure of the lane region, on the other hand, is different in the two situations. For situation (A) the corresponding snapshot in Figure 1 reveals fixed lattice points while the snapshot in Figure 2 situation (B) shows a network-like structure. For situation (A), an initial configuration with lanes placed on a square lattice separated from a completely depleted region is stable in simulations, as well. Thus, we assume that in situation (A) the lanes/no-lanes phase is a transient state toward a complete square lattice and no-lane phase separation. Hydrodynamic interactions destroy the coexistence phase for $\phi = 0.01$. It only occurs in a denser system with $\phi = 0.1$ whereas in situation (A) this state shows already up at $\phi = 0.01$. Additionally, the voids are more pronounced in the latter case compared to

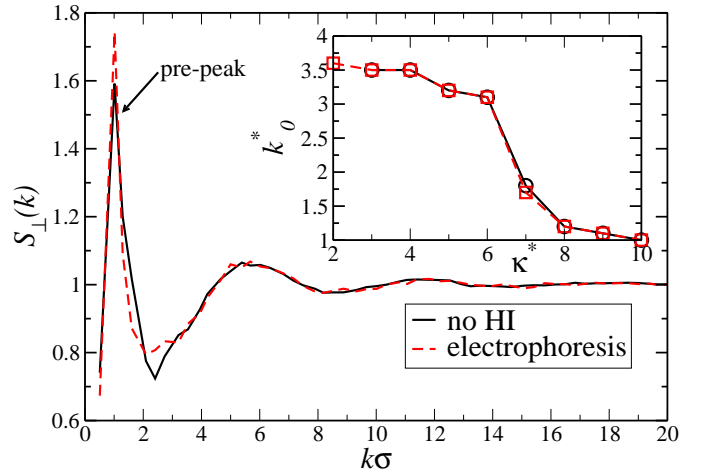


Fig. 4. Partial structure factor $S_{\perp}(k)$ of like-charged particles perpendicular to the driving field for $\kappa^* = 10$ and $\phi = 0.1$ for hydrodynamics neglected and electrophoresis. The pre-peak at $k_0^* = k_0\sigma$ indicates an additional length scale of the structure in the network-like phase. The inset shows the position k_0^* of the pre-peak as a function of the inverse screening length κ^* for a fixed volume fraction of $\phi = 0.1$.

situation (B). Upon increasing $\kappa^* \geq 2$ for $\phi = 0.1$ in both situations we find a network-like structure whose characteristic spacing is increasing with increasing κ^* . For situation (A) there is also a small coexistence region between network and square lattice at $\kappa^* = 2$.

To obtain a quantitative measure of the characteristic spacing in the network structure, we determine a structure factor perpendicular to the driving field of like-charged particles. The steady-state partial structure factor has been calculated by evaluating the expression

$$S_{\perp}(k) = 1 + \rho \hat{h}_{\perp}(k), \quad (12)$$

with $\rho = 6\phi/\pi\sigma^3$ the number density and the wave vector $k = |\mathbf{k}|$, where $\mathbf{k} = (2\pi/l)(n_x, n_y)$ and n_x, n_y are integers. $\hat{h}_{\perp}(k)$ is the Fourier transform of the total correlation function $h_{\perp}(\mathbf{r}_{\perp}) = g_{\perp}(\mathbf{r}_{\perp}) - 1$ with $\mathbf{r} = (\mathbf{r}_{\perp}, z)$ and

$$g_{\perp}(r_{\perp}) = \frac{1}{\rho N} \left\langle \sum_{\substack{i,j, i \neq j \\ (z_i = z_j)}}^{2N} \delta(\mathbf{r}_{\perp} - |\mathbf{r}_{\perp i} - \mathbf{r}_{\perp j}|) \delta(z_i - z_j) \right\rangle_t, \quad (13)$$

where $\delta(\mathbf{x})$ denotes Dirac's delta distribution. An example of the steady-state partial structure factors for $\kappa^* = 10$ and $\phi = 0.1$ for both situation, (A) and (B), is shown in Figure 4. One clearly observes a pronounced pre-peak at the wave number k_0 in both cases. A pre-peak in the structure factor is an indication of an additional ‘‘mesoscopic’’ length scale, *i.e.*, a length scale which is significantly larger than a microscopic length scale. This is also typical for bicontinuous networks, such as, *e.g.*, microemulsions [42, 43]. In the inset we additionally present the position k_0 of the pre-peak as a function of the inverse screening length. It

is evident from the picture that the characteristic spacing is indeed growing with increasing κ^* . In the limit of $\kappa^* \rightarrow \infty$ the particles' interaction reduces to the repulsive soft core equation (2). For such a system it is anticipated that the ultimate steady state is a phase-separated one [10]. Therefore, we assume that for strongly screened particles k_0 remains constant and corresponds to a characteristic spacing of half of the box length. We find hardly any difference between situation (A) and (B).

For $\phi = 0.2$ an additional phase for small inverse screening length shows up in both phase diagrams. Oppositely driven lanes are placed on a square lattice with an alternating charge pattern. The formation of this lattice structure can be qualitatively understood from an effective interaction between oppositely charged driven lanes which has a short-ranged repulsive and a long-ranged attractive interaction. The former stems from the friction between oppositely driven particles, while the later results from the Coulomb interaction. The square lattice then reduces the electrostatic energy of the system because each particle has only oppositely charged neighbors. For increasing salt concentrations we encounter a coexistence region between the square lattice and the network-like phase and finally end up in a pure network-like phase. The phase diagram is in both situations very similar, only the borders of the transitions are slightly shifted. In the electrophoresis case the network-like structure is preferred to the square lattice.

For a higher volume fractions of $\phi = 0.3$ a coexistence regime between a triangular lattice and a network-like structure is found. The lattice points in the triangular phase are rather randomly decorated with different charges. Here, the short-range repulsion plays the dominant role compared to the electrostatic interaction. It enforces a triangular lattice due to packing effects although electrostatically it is strongly disfavored because like-charged particles necessarily occupy lattice points next to each other. Again, hydrodynamic interactions slightly shift the phase boundaries towards the network-like structure.

For the highest volume fraction studied, $\phi = 0.4$, both phase diagrams show exactly the same behavior. Here, the short-range repulsions dictate the phase behavior for nearly all salt concentration but for $\kappa^* = 1$ and enforces lanes to be placed on a triangular lattice. Only for $\kappa^* = 1$, where electrostatic interactions are prominent, a square lattice is preferred. In principle a square lattice is possible up to the packing of a simple cubic lattice of $\phi = 0.52$.

In summary we observe very similar behavior in both situations. The observed differences can be qualitatively explained by the fact that hydrodynamic interactions disfavor lanes driven oppositely past each other.

3.3 Sedimentation

Regarding sedimentation, Figure 3, the whole phase diagram exhibits *only* three different phases. For volume fractions $\phi \leq 0.1$ we do not find lane formation for all inverse screening length studied. For increasing volume

fractions and strong electrostatic interactions, $\kappa^* \leq 2$, first the square lattice at $\phi \approx 0.3$, that is also present in the previous two situations, is recovered and then the system reenters a region with no-lanes for $\phi = 0.4$. This behavior nicely illustrates the competition between hydrodynamic interactions disfavoring lanes driven oppositely past each other and the electrostatic interactions favoring a square lattice. Only for the small regime around $\phi \approx 0.3$ the electrostatics succeeds the hydrodynamic interactions and enforces a square lattice. For all other volume fractions laning is destroyed. However, for stronger salt concentrations, where the Coulombic coupling is reduced, we discover a situation that is not present in the previous situations (A) and (B), namely a region in which only two big completely separated lanes. We call this state *phase separated*. In that case the long-ranged hydrodynamic interactions prescribe the structure and the short-ranged Yukawa interaction plays its role only at the rough interface of the two phases. From our simulations we conclude the lanes are separated by half of the box length.

3.4 Drift velocity

Now, we study the influence of hydrodynamic interaction on the drift velocity along the field direction that is defined as follows:

$$v^2 := \lim_{t \rightarrow \infty} \frac{\langle [(\mathbf{r}_i(t) - \mathbf{r}_i(0)) \cdot \mathbf{e}_z]^2 \rangle}{t^2}. \quad (14)$$

This entity measures the mean-square displacement of each particle in the nonequilibrium steady-state. A study on the effect of hydrodynamics on the drift velocity of like-charged colloidal particles was carried out by Watzlawek and Nägele [44]. We study two cases, first we fix the volume fraction at $\phi = 0.3$ and vary the inverse screening length and afterward vice versa for $\kappa^* = 1$.

In Figure 5 we display $v^* = v/v_0$, where $v_0 = 150\sigma/\tau_B$ is the drift velocity of an infinitely diluted system, for a fixed volume fraction $\phi = 0.3$ as a function of the inverse screening length κ^* for all three situations. For all cases the drift velocity increases with decreasing Coulomb coupling because oppositely charged colloids attract each other while driven in opposite direction and lanes mutually retard each other. For very strongly screened particles where this friction is less important all three curves reveal approximately the same value of $v \approx 0.87$. Accordingly, this value is close to the drift velocity v_0 an isolated particle subjected to the same driving force. While in (A) and (B) v grows gradually, in the sedimentation curve we encounter a jump in the drift velocity between $\kappa^* = 3$ and $\kappa^* = 4$. This coincides with the transition from the no-lane regime to the phase separated regime, see the phase diagram Figure 3. On the other hand for $\kappa^* \leq 2$, where we find a square lattice, the drift velocity is similar to $\kappa^* = 3$. From that we conclude that the phase-separated state of lanes supports particle transport, while lanes placed on a square lattice enforced by strong Coulombic interactions slow down particle transportation.

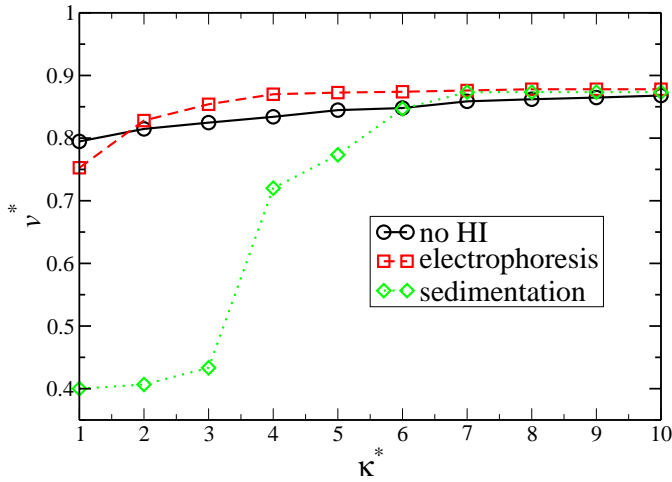


Fig. 5. Average dimensionless drift velocity $v^* = v/v_0$ in drive direction as a function of the inverse screening length κ^* at $\phi = 0.3$ for Brownian-dynamics simulations with hydrodynamic interactions neglected, taken into account through μ_{ij}^{LA} , and μ_{ij}^{RP} .

A further interesting feature is that curves for (A) and (B) intersect between $\kappa^* = 1$ and $\kappa^* = 2$ and that the screened hydrodynamic interaction enhance the drift velocity for larger inverse screening length. The same is true for the unscreened hydrodynamic interactions in the sedimentation for $\kappa^* \geq 6$. When studying the drift velocity for a fixed inverse screening length but for varying volume fractions in Figure 6 we find again an intersection point of the curves for situations (A) and (B). Here, the drift velocity in the electrophoresis reaches an approximately constant value of $v^* \approx 0.75$ for $\phi = 0.1-0.4$, whereas it gradually decreases when hydrodynamic interactions are neglected. For the sedimentation the drift velocity decreases monotonically. In contrast to the case of varying salt concentration we do not encounter a jump in the sedimentation drift velocity when entering the square lattice at $\phi = 0.3$ and re-entering the no-lane regime at $\phi = 0.4$.

4 Conclusions

In conclusion the influence of hydrodynamic interactions on lane formation of opposite charged colloids driven by an electric field or by gravity was investigated by Brownian-dynamics computer simulations. Hydrodynamic interactions were included on the Rotne-Prager level. For an electric field, the leading Oseen term is screened due to the presence of counterions. The latter fact has led to more similar steady-state phase diagrams for an electric field as a driving source than that in the simple case of neglected hydrodynamic interactions. Various steady state were obtained as a function of the colloidal density and the range of the interaction. They can qualitatively be understood in terms of a competition of the mutual Coulomb attraction and friction of sliding lanes. At high densities the

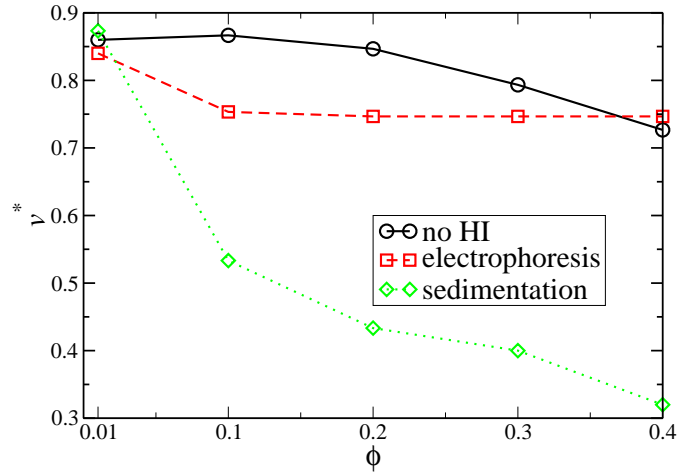


Fig. 6. Average dimensionless drift velocity $v^* = v/v_0$ in drive direction as a function of the volume fractions ϕ at $\kappa^* = 1$ for Brownian-dynamics simulations with hydrodynamic interactions neglected, taken into account through μ_{ij}^{LA} , and μ_{ij}^{RP} .

lateral structure is crystalline, the crystal is either triangular as dictated by packing at high densities and high screening or square-like at low-screening which minimizes the Coulomb attractive energy. On the other hand, in sedimentation where the two colloidal species have the same buoyant mass up to a relative sign, friction of sliding lanes is strongly enhanced leading to macroscopic separation of lanes.

The steady-state phase diagram can in principle be verified in real-space experiments of charged suspensions which are driven in an electric field or sedimenting [22]. It would be interesting to construct a microscopic theory for the lane transitions which includes the lateral crystalline structure. The instability analysis within a dynamical density functional theory as applied to the case of equal charges in two spatial dimensions [12,45] should in principle be generalizable to the case of oppositely charged particles.

Finally more sophisticated simulations schemes are needed in order to go beyond the Rotne-Prager level of approximation used in this paper. Among the various promising approaches are the stochastic rotation dynamics code [46,47], a lattice Boltzmann theory including hydrodynamics [48–52] and counterion flow or the recently developed fluid particle dynamics methods [53–55].

We thank M. Leunissen, A. van Blaaderen, R. Yamamoto, A. Louis, and J. Padding for helpful remarks and the DFG (SFB TR6, project section D1) and the Graduiertenförderung of the Heinrich-Heine-Universität Düsseldorf for financial support.

References

1. P.N. Pusey, in *Liquids, Freezing and Glass Transition*, edited by J.P. Hansen, D. Levesque, J. Zinn-Justin (North-Holland, Amsterdam, 1991).

2. H. Löwen, J.P. Hansen, J.N. Roux, *Phys. Rev. A* **44**, 1169 (1991).
3. G. Nägele, *Phys. Rep.* **272**, 215 (1996).
4. J. Vermant, M.J. Solomon, *J. Phys.: Condens. Matter* **17**, R187 (2005).
5. R. Pesché, G. Nägele, *Europhys. Lett.* **51**, 584 (2000).
6. S. Katz, J.L. Lebowitz, H. Spohn, *Phys. Rev. B* **28**, 1655 (1983).
7. S. Katz, J.L. Lebowitz, H. Spohn, *J. Stat. Phys.* **34**, 497 (1984).
8. B. Schmittmann, R.K.P. Zia, *Statistical Mechanics of Driven Diffusive Systems* (Academic Press, London, 1995).
9. H. Löwen, *J. Phys.: Condens. Matter* **13**, R415 (2001).
10. J. Dzubiella, G.P. Hoffmann, H. Löwen, *Phys. Rev. E* **65**, 021402 (2002).
11. R.R. Netz, *Europhys. Lett.* **63**, 616 (2003).
12. J. Chakrabarti, J. Dzubiella, H. Löwen, *Europhys. Lett.* **61**, 415 (2003).
13. H. Löwen, J. Dzubiella, *Faraday Discuss.* **123**, 99 (2003).
14. J. Delhomme, *Phys. Rev. E* **71** (1), 016705 (2005).
15. R.B. Pandey, J.F. Gettrust, R. Seyfarth, L.A. Cueva-Parra, *Int. J. Mod. Phys. C* **14** (7), 955 (2003).
16. M. Köppl, P. Henseler, A. Erbe, P. Nielaba, P. Leiderer, *Phys. Rev. Lett.* **97**, 208302 (2006).
17. R. Jiang, D. Helbing, P.K. Shuklai, Q.S. Wu, *Physica A* **368**, 567 (2006).
18. R. Kolbl, D. Helbing, *N. J. Phys.* **5**, 48 (2003).
19. G.C.M.A. Ehrhardt, A. Stephenson, P.M. Reis, *Phys. Rev. E* **71**, 041301 (2005).
20. M.P. Ciamarra, A. Coniglio, M. Nicodemi, *Phys. Rev. Lett.* **94**, 188001 (2005).
21. G.K. Batchelor, R.W.J. van Rensburg, *J. Fluid Mech.* **166**, 379 (1986).
22. M.E. Leunissen, C.G. Christova, A.P. Hynninen, C.P. Royall, A.I. Campbell, A. Imhof, M. Dijkstra, R. van Roij, A. van Blaaderen, *Nature* **437**, 235 (2005).
23. A.P. Hynninen, M.E. Leunissen, A. van Blaaderen, M. Dijkstra, *Phys. Rev. Lett.* **96** (1), 018303 (2006).
24. A.P. Hynninen, C.G. Christova, R. van Roij, A. van Blaaderen, M. Dijkstra, *Phys. Rev. Lett.* **96** (13), 138308 (2006).
25. M. Rex, H. Löwen, *Phys. Rev. E* **75**, 051402 (2007).
26. D. Long, A. Ajdari, *Eur. Phys. J. E* **4**, 29 (2001).
27. C.P. Royall, M.E. Leunissen, A.P. Hynninen, M. Dijkstra, A. van Blaaderen, *J. Chem. Phys.* **124**, 2447061 (2006).
28. E. Allahyarov, H. Löwen, S. Trigger, *Phys. Rev. E* **57**, 5818 (1998).
29. D.L. Ermak, J.A. McCammon, *J. Chem. Phys.* **69**, 1352 (1978).
30. M.P. Allen, D.J. Tildesley (Editors), *Computer Simulation of Liquids* (Clarendon Press Oxford, Oxford, 1989).
31. E. Wajnryb, P. Szymczak, B. Cichocki, *Physica A* **335**, 339 (2004).
32. J. Rotne, S. Prager, *J. Chem. Phys.* **50**, 4831 (1969).
33. L. Durlofsky, J.F. Brady, G. Bossis, *J. Fluid Mech.* **180**, 21 (1987).
34. A.J.C. Ladd, *J. Chem. Phys.* **88**, 5051 (1988).
35. B. Cichocki, B.U. Felderhof, K. Hinsen, E. Wajnryb, J. Bliawdziewicz, *J. Chem. Phys.* **100**, 3780 (1994).
36. A. Sierou, J.F. Brady, *J. Fluid Mech.* **448**, 115 (2001).
37. A.J. Banchio, J.F. Brady, *J. Chem. Phys.* **118**, 10323 (2003).
38. E.R. Smith, I.K. Snook, W. van Meegen, *Physica A* **143**, 441 (1987).
39. E.R. Smith, *Faraday Discuss. Chem. Soc.* **83**, 193 (1987).
40. J.F. Brady, R.J. Phillips, J.C. Lester, G. Bossis, *J. Fluid Mech.* **195**, 257 (1988).
41. C.W.J. Beenakker, *J. Chem. Phys.* **85**, 1581 (1986).
42. M. Teubner, R. Strey, *J. Chem. Phys.* **87**, 3195 (1987).
43. G. Gompper, M. Schick, *Phys. Rev. Lett.* **62**, 1647 (1989).
44. M. Watzlawek, G. Nägele, *J. Colloid Interface Sci.* **214**, 170 (1999).
45. J. Chakrabarti, J. Dzubiella, H. Löwen, *Phys. Rev. E* **70**, 012401 (2004).
46. J.T. Padding, A.A. Louis, *Phys. Rev. E* **74**, 031402 (2006).
47. J.T. Padding, A.A. Louis, *Phys. Rev. Lett.* **93**, 220601 (2004).
48. V. Lobaskin, B. Dünweg, *N. J. Phys.* **6**, 54 (2004).
49. A. Chatterji, J. Horbach, *J. Chem. Phys.* **122**, 184903 (2005).
50. F. Capuani, I. Pagonabarraga, D. Frenkel, *J. Chem. Phys.* **124**, 124903 (2006).
51. A. Chatterji, J. Horbach, *J. Chem. Phys.* **126**, 064907 (2007).
52. V. Lobaskin, B. Dünweg, M. Medebach, T. Palberg, C. Holm, *Phys. Rev. Lett.* **98**, 176105 (2007).
53. H. Kodama, K. Takeshita, T. Araki, H. Tanaka, *J. Phys.: Condens. Matter* **16**, L115 (2004).
54. K. Kim, Y. Nakayama, R. Yamamoto, *Phys. Rev. Lett.* **96**, 208302 (2006).
55. K. Kim, R. Yamamoto, *Macromol. Theory Simul.* **14**, 278 (2005).